ResearchGate

See discussions, stats, and author profiles for this publication at: https://www.researchgate.net/publication/51627399

Ultrastructural and Mineral Phase Characterization of the Bone-Like Matrix Assembled in F-OST Osteoblast Cultures

ARTICLE *in* CALCIFIED TISSUE INTERNATIONAL · SEPTEMBER 2011

Impact Factor: 3.27 · DOI: 10.1007/s00223-011-9526-9 · Source: PubMed

CITATIONS
8

READS
38

9 AUTHORS, INCLUDING:

Andre Rossi
Centro Brasileiro de Pesquisas Físicas
18 PUBLICATIONS **81** CITATIONS
SEE PROFILE

Rosane San Gil
Federal University of Rio de Janeiro
71 PUBLICATIONS **434** CITATIONS
SEE PROFILE

Radovan Borojevic
Petrópolis Faculty of Medicine
373 PUBLICATIONS **5,860** CITATIONS
SEE PROFILE

Alex Balduino
Excellion Biomedical Services, Amil / Unite…
34 PUBLICATIONS **446** CITATIONS
SEE PROFILE

Available from: Radovan Borojevic
Retrieved on: 16 January 2016

Calcif Tissue Int (2011) 89:358–371
DOI 10.1007/s00223-011-9526-9

ORIGINAL RESEARCH

Ultrastructural and Mineral Phase Characterization of the Bone-Like Matrix Assembled in F-OST Osteoblast Cultures

W. Querido · L. G. Abraçado · A. L. Rossi · A. P. C. Campos · A. M. Rossi · R. A. S. San Gil · R. Borojevic · A. Balduino · M. Farina

Received: 29 July 2011 / Accepted: 4 August 2011 / Published online: 7 September 2011
© Springer Science+Business Media, LLC 2011

Abstract Cell cultures are often used to study bone mineralization; however, not all systems achieve a bone-like matrix formation. In this study, the mineralized matrix assembled in F-OST osteoblast cultures was analyzed, with the aim of establishing a novel model for bone mineralization. The ultrastructure of the cultures was investigated using scanning electron microscopy, atomic force microscopy, and transmission electron microscopy (TEM). The mineral phase was characterized using conventional and high-resolution TEM, energy-dispersive X-ray spectroscopy, X-ray diffraction, Fourier transform infrared spectroscopy, and solid-state ^{31}P and ^{1}H nuclear magnetic resonance. F-OST osteoblast cultures presented a clear nodular mineralization pattern. The chief features of the mineralizing nodules were globular accretions ranging from about 100 nm to 1.5 μm in diameter, loaded with needle-shaped crystallites. Accretions seemed to bud from the cell membrane, increase in size, and coalesce into larger ones. Arrays of loosely packed, randomly oriented collagen fibrils were seen along with the accretions. Mineralized fibrils were often observed, sometimes in close association with accretions. The mineral phase was characterized as a poorly crystalline hydroxyapatite. The Ca/P atomic ratio was 1.49 ± 0.06. The presence of OH was evident. The lattice parameters were $a = 9.435$ Å and $c = 6.860$ Å. The average crystallite size was 20 nm long and 10 nm wide. Carbonate substitutions were seen in phosphate and OH sites. Water was also found within the apatitic core. In conclusion, F-OST osteoblast cultures produce a bone-like matrix and may provide a good model for bone mineralization studies.

Keywords Osteoblast · In vitro model · Bone · Biological apatite · Biomineralization

The authors have stated that they have no conflict of interest.

W. Querido · L. G. Abraçado · A. L. Rossi · R. Borojevic · M. Farina
Instituto de Ciências Biomédicas, Universidade Federal do Rio de Janeiro, Rio de Janeiro, RJ 21941-902, Brazil

W. Querido
Instituto de Biofísica Carlos Chagas Filho, Universidade Federal do Rio de Janeiro, Rio de Janeiro, RJ 21941-902, Brazil

A. P. C. Campos
Divisão de Metrologia de Materiais, Instituto Nacional de Metrologia, Normalização e Qualidade Industrial, Duque de Caxias, RJ 25250-020, Brazil

A. M. Rossi
Grupo de Biomateriais: Preparação, Caracterização, Modelagem Teórica e Aplicações Biomédicas, Centro Brasileiro de Pesquisas Físicas, Rio de Janeiro, RJ 22290-180, Brazil

R. A. S. San Gil
Laboratório Multiusuário de RMN de Sólidos Professora Adelina Costa Neto, Universidade Federal do Rio de Janeiro, Rio de Janeiro, RJ 21941-909, Brazil

A. Balduino
Centro de Terapia Celular e Bioengenharia Ortopédica, Instituto Nacional de Traumatologia e Ortopedia, Rio de Janeiro, RJ 20230-024, Brazil

M. Farina (✉)
Centro de Ciências da Saúde, Instituto de Ciências Biomédicas, Universidade Federal do Rio de Janeiro, Av. Carlos Chagas Filho, 373, bloco F, sala F2-027, Cidade Universitária, Rio de Janeiro, RJ 21941-902, Brazil
e-mail: mfarina@anato.ufrj.br

Bone matrix can be defined as a composite material in which a mineral phase is deposited into an organic framework [1, 2]. Type I collagen fibrils are the major component of this framework, which also contains many noncollagenous matrix proteins (NCPs), such as bone sialoprotein (BSP) and osteopontin (OPN) [1, 3]. The mineral found in bone comprises a highly substituted, nanostructured hydroxyapatite, described as poorly crystalline, nonstoichiometric, containing carbonate and HPO_4, and deficient in Ca and OH [2, 4]. The chemical formula of stoichiometric hydroxyapatite is $Ca_{10}(PO_4)_6(OH)_2$; however, bone apatite may be better represented by the following (where □ spaces are structural vacancies) [5]:

$$Ca_{8.3}\square_{1.7}(PO_4)_{4.3}(CO_3 \text{ and } HPO_4)_{1.7}(OH \text{ and } 0.5CO_3)_{0.3}\square_{1.7}$$

The composition of bone apatite is, however, much more variable than presented in the above formula, accepting many other ionic substitutions, such as Na, Mg, K, and Sr replacing Ca as well as Cl and F replacing OH [2]. Structural water is also present in bone apatite [6]. Moreover, the surface hydrated layers (nonapatitic environment) proposed for bone apatite [5] and the crystallite core (apatitic lattice) were shown to present distinct compositions, such as the former having relatively higher amounts of Mg and HPO_4 [7]. The composition of bone apatite also varies during maturation, reflecting the gradual decrease in the hydrated surface layer associated with an increase in the crystallite core [5, 7]. Thus, it is not an easy task to determine an overall chemical formula for bone apatite.

Bone mineralization may occur by different mechanisms, mainly related to matrix vesicles, NCP, and/or collagen fibrils. Matrix vesicles are membrane-invested, globular structures of about 10–200 nm in diameter in which apatite nucleation occurs [8, 9]. Some NCPs can also regulate mineral deposition; they may form globular aggregates ranging about 300–800 nm in diameter and are often associated with the so-called crystal ghosts [10, 11]. Matrix vesicles and NCP aggregates may increase in size and coalesce, creating larger, mineralized globular accretions [11, 12]. The collagen fibrils are the ultimate framework in which mineralization occurs [8, 13]. The organic framework and mineralization mechanisms change along bone development. Immature woven bone presents poorly oriented collagen fibrils and a relatively higher content of NCP, and its chief mineralization features are related to matrix vesicles and NCP; mature lamellar bone displays ordered sheets of collagen fibrils and a relatively lower content of NCP, and its main features are related to collagen fibrils [1, 3, 14].

The development of experimental models for bone mineralization studies is of great interest not only in bone biology but also in biomaterial and bone engineering research. Osteoblastic cell cultures are often used to provide such models [11, 15–18]; however, not all culture systems achieve a bone-like mineralization [15, 19, 20]. Moreover, the traditional use of β-glycerophosphate in the osteogenic culture medium may induce a nonphysiological, dystrophic mineralization if it does not occur on a proper matrix [18, 21]. Nevertheless, the characterization of the matrix and mineral phase produced in culture systems is often ignored, relying mainly on nonspecific staining methods [18, 21], such as von Kossa's [19].

The cells used in this study were F-OST osteoblasts, previously isolated from the endosteal region of adult BALB/c mice femurs [22]. F-OST stands for *femur-osteoblasts*. The cells were harvested from bone fragments free of periosteal and marrow tissue using a two-step collagenase treatment and characterized phenotypically and functionally as mature osteoblasts with a tendency to terminally differentiate. They were shown to produce several typical bone matrix proteins, such as type I collagen, BSP, and OPN. Moreover, the cells presented high alkaline phosphatase activity and spontaneously formed extensive mineralizing nodules when cultured under basal conditions. The main goal of the present work was to characterize the ultrastructure and mineral phase of the matrix assembled in F-OST osteoblast cultures, with the of aim establishing a novel model for studies of bone mineralization.

Materials and Methods

Cell Culture

F-OST osteoblasts [22] were cultured in Dulbecco's modified Eagle medium (DMEM) containing 10% fetal bovine serum (FBS) and antibiotics (100 U/ml penicillin and 100 μg/ml streptomycin) at 37°C in a humidified 5% CO_2 incubator. Members of our group are currently characterizing F-OST osteoblasts as a cell line that maintains alkaline phosphatase activity, collagen synthesis, and formation of extensive mineralizing nodules at least up to passage 25. In this study, cells were used after 6–8 passages. For the mineralization assay, cells were seeded at a density of $1.3 \times 10^4/cm^2$ and, once semiconfluence was reached, cultured in the presence of 50 μg/ml ascorbic acid and 10 mM β-glycerophosphate to accelerate matrix and mineral formation [18, 21].

Staining Methods

Cells were cultured in 24-well plates for 7, 14, 21, and 28 days; rinsed with phosphate-buffered saline (PBS), and fixed in 4% paraformaldehyde for 30 min, followed by three

5-min washes with PBS. Phosphate deposits were shown in black using von Kossa's method. Briefly, cultures were exposed to a 2% silver nitrate solution under sunlight for 20 min and washed with distilled water. Unreacted silver salts were dissolved with a 5% sodium thiosulfate solution and washed off with distilled water. The presence of calcium in the mineralized matrix was determined by staining in red with an acid nuclear fast red–saturated solution for 40 min, followed by washes in distilled water. All samples were air-dried and observed in an Olympus (Tokyo, Japan) IX71 optical microscope equipped with a DP71 CCD camera. Although these staining methods alone are not sufficient to characterize a bone-like matrix [19], they are essential in the initial investigation of the cultures. Whole-well images of the nuclear fast red–stained cultures were analyzed using Image-Pro Plus software (version 6.0; Media Cybernetics, Silver Spring, MD) in order to quantify the mineralized area. Briefly, thresholding of the gray-scale images was performed, creating a binary image in which the mineralized surface could be estimated as a percentage of total culture area. Statistical analyses were performed with the InStat software (version 3.0; GraphPad, San Diego, CA). One-way analysis of variance (ANOVA) followed by Tukey-Kramer multiple comparisons test was used to compare groups, and differences were considered significant when $P < 0.05$.

Scanning Electron Microscopy

Cells were cultured on 13-mm^2 glass coverslips in 24-well plates for 28 days, rinsed with warm PBS, and fixed in 2.5% glutaraldehyde in 0.1 M sodium cacodylate buffer (Na-caco) for 60 min, followed by three 10-min washes with Na-caco. Cultures were then postfixed in 1% osmium tetroxide in 0.1 M Na-caco for 20 min and washed three more times. Afterward, cultures were dehydrated in 10-min baths with a graded ethanol series (35, 50, 70, 80, 90%, and twice with 100% ethanol) and critical point–dried using CO_2 in a Balzers (Balzers, Liechtenstein) CPD 020. Coverslips were attached to stubs, and cultures were finally sputter-coated with gold in a Bal-Tec (Balzers, Liechtenstein) SCD 050 and observed in a FEI (Eindhoven, the Netherlands) Quanta 250, a JEOL (Tokyo, Japan) 5310, or a JEOL JSM-6460LV microscope at 25, 30, and 20 kV, respectively.

Atomic Force Microscopy

Cells were cultured and processed as described for scanning electron microscopy (SEM), without the gold coating step. Since the fully mineralized cultures presented a high surface relief, often causing the cantilever and tip to oscillate with extreme amplitude and collide against the samples, they were partially decalcified in sequential baths with 10% EDTA solution, followed by washes with distilled water, to facilitate analysis. Cultures were examined in a NT-MDT (Moscow, Russia) NTEGRA microscope operating in semicontact mode. Height images were acquired, highlighting the topographic features of the cultures. Roughness analysis and bearing ratio were obtained using Nova software (version 1.0.26; NT-MDT).

Mineral Extraction

Cells were cultured in 75-cm^2 flasks for 28 days and rinsed with distilled water. The mineral was extracted by removal of the organic portion based on methods found not to alter the mineral phase [23, 24]. The possible effect of the extraction procedure on the dissolution of some amorphous mineral phases and labile groups is considered in the "Discussion" section. Briefly, cultures were exposed to a 5% sodium hypochlorite solution for about 10 min in continuous motion in a vortex mixer, followed by centrifugation of the resultant suspension at 14,000 rpm for 2 min in an Eppendorf (Hamburg, Germany) 5415C microcentrifuge. The extracted mineral pellets were then washed three times with Milli-Q water (Millipore, Billerica, MA) and twice with 100% ethanol and dried overnight at 40°C.

Transmission Electron Microscopy

Cells were cultured in 24-well plates for 28 days and fixed, postfixed, and dehydrated as described for SEM. Afterward, cultures were embedded in Spurr resin by slow infiltration in baths of graded resin series in ethanol (1:2, 1:1, 2:1, and twice with pure resin) and polymerization at 70°C overnight. Ultrathin transverse sections of about 80 nm were made using a diamond knife in a RMC (Tucson, AZ) Power Tome X ultramicrotome and deposited on Formvar-coated transmission electron microscopy (TEM) copper grids. Sections were then stained with uranyl acetate for 20 min and lead citrate for 3 min, rinsed with distilled water, and observed in an FEI Tecnai G^2 Bio TWIN microscope at 200 kV. For observation of the mineral phase, the extracted mineral was subjected to an additional procedure [23]. Briefly, about 1 mg of extracted mineral was mixed with 1.5 ml of 2.5% sodium hypochlorite and sonicated for 10 min. Afterward, the suspension was allowed to settle for 2 min and the supernatant was recovered and centrifuged at 14,000 rpm for 2 min in an Eppendorf 5415C microcentrifuge. The pellets were then washed three times with Milli-Q water and twice with 95% ethanol, resuspended in about 200 µl of 100% ethanol, and further sonicated. About 2 µl of the just-sonicated mineral suspension was deposited on Formvar-coated TEM copper grids, air-dried, and observed in a JEOL 1200EX microscope at 100 kV.

High-Resolution TEM

A small aliquot of the extracted mineral was mixed with 100% ethanol and sonicated. About 2 µl of the suspension was then deposited on a Ted Pella (Redding, CA) ultrathin carbon film supported by a lacey carbon film on a 400 mesh copper grid, air-dried, and observed in a JEM 3010 URP microscope at 300 kV. To identify the observed mineral phase, the FFT patterns of the crystalline domains found in high-resolution TEM (HRTEM) images were analyzed using DigitalMicrograph software (version 1.7; Gatan, Pleasanton, CA) bundled with the DiffTools plug-in, version 3.1. The interplanar distances and relative angles found for the representative diffraction spots were compared with values assigned to hexagonal hydroxyapatite with lattice parameters $a = 9.418$ Å and $c = 6.884$ Å (ICDD PDF 9-432). The zone axis was confirmed using the JEMS software package (version 3.38; CIME-EPFL, Lausanne, Switzerland).

Energy-Dispersive X-Ray Spectroscopy

Samples were prepared as described for HRTEM, using formvar-coated TEM copper grids. The mineral was analyzed in an FEI Titan 80-300 microscope at 300 kV equipped with an EDAX energy-dispersive X-ray spectroscopy (EDS) System. Fifteen measurements were performed. The Ca/P atomic ratio was averaged by semi-quantitative automated analysis using TEM Imaging & Analysis software (version 3.2, FEI). Briefly, the atomic percent of the elements was estimated based on the integrated intensities of the peaks, found after background subtraction and spectrum fitting.

X-Ray Powder Diffraction

About 50 mg of the extracted mineral was analyzed in a PANalytical (Almelo, the Netherlands) X'Pert PRO diffractometer using CuK_α radiation ($\lambda = 1.5418$ Å). The X-ray powder diffraction (XRD) pattern was recorded from 20° to 45° 2θ with a step size of 0.02° 2θ and counting time of 5 s/step and analyzed using OriginPro software (version 8; OriginLab, Northampton, MA). To identify the mineral phase, the diffraction angles 2θ for the observed peaks were used to determine the interplanar distances d_{hkl} following Bragg's law (where hkl refers to Miller indices):

$$2d_{hkl} \sin\theta = n\lambda$$

where the order of reflection n is an integer set to 1 for indexing XRD patterns and determining the nature and crystal structure of minerals. The d_{hkl} values, in conjunction with the relative intensities of the diffraction peaks, were compared to standard values from the powder diffraction files (PDFs) for several minerals available in the International Centre for Diffraction Data (ICDD) PDF-2 database. The unit cell lattice parameters a and c were determined using d_{hkl} values found, respectively, for the (310) and (002) reflections, employing the equation for crystal structures with hexagonal symmetry [25]:

$$1/d_{hkl}^2 = (4/3)(h^2 + hk + k^2)/a^2 + l^2/c^2$$

Crystallinity was qualified based on peak broadening and resolution. Average crystallite size τ was estimated based on the full widths at half-maximum $\beta_{1/2}$ (values in radians) of the reflections (002) for length along the c-axis and (310) for width perpendicular to the c-axis, using Scherrer's equation with $K = 0.9$ [26]:

$$\tau = K\lambda/\beta_{1/2} \cos\theta$$

Fourier Transform Infrared Spectroscopy

About 1 mg of the extracted mineral was mixed with 100 mg of finely grinded KBr, pressed into a thin translucent disc at 8 Ton/cm^2 for 8 min and analyzed in a Shimadzu (Kyoto, Japan) IRPrestige-21 spectrometer. Fourier transform infrared spectroscopy (FTIR) absorption spectra were recorded from 4,000 to 400 cm^{-1} at a resolution of 4 cm^{-1}, averaging 128 scans and analyzed using the Shimadzu IR Solution software, version 1.4. The $\nu_2CO_3^{2-}$ domain (890–850 cm^{-1}) was further acquired with a resolution of 1 cm^{-1}, more suitable for a detailed investigation of the short spectral region. Atmosphere correction and baseline multipoint alignment were performed. To enhance the resolution of overlapping peaks in the $\nu_3PO_4^{3-}$ (1,200–900 cm^{-1}), $\nu_3CO_3^{2-}$ (1,600–1,350 cm^{-1}), and $\nu_2CO_3^{2-}$ (890–850 cm^{-1}) domains, the spectral regions were deconvoluted. The deconvolution parameters were adjusted for each analyzed domain, comprising an apodization function, the half-width of the band, and the optical path length for deciding the effective range of the interferogram. A Bessel function was chosen for all domains. For the $\nu_3PO_4^{3-}$ domain, the band width was 20 cm^{-1} and the path length was 0.1 cm^{-1}; for the $\nu_3CO_3^{2-}$ domain, the band width was 15 cm^{-1} and the path length was 0.1 cm^{-1}; and for the $\nu_2CO_3^{2-}$ domain, the band width was 7 cm^{-1} and the path length was 0.2 cm^{-1}. Spectra were manipulated to obtain the best resolution enhancement without causing overdeconvolution. The mineral was identified based on peak assignment and band shapes as previously described [7, 27, 28].

Solid-State ^{31}P And ^{1}H Nuclear Magnetic Resonance

About 50 mg of the extracted mineral was analyzed on a Bruker (Rheinstetten, Germany) AVANCE III 400

spectrometer (9.4 T), operating at Larmor frequencies of 161.9 MHz for ^{31}P and 400.0 MHz for ^{1}H. The sample was packed into a 4-mm magic-angle spinning (MAS) zirconia rotor with Kel-F caps and spun at 12 kHz for ^{31}P and 10 kHz for ^{1}H, using a Bruker 4 mm cross-polarization (CP)/MAS probe. All data were collected at ambient temperature. For ^{31}P analysis, a Bloch decay sequence (single-pulse excitation) with high-power proton decoupling was used, with a 90° pulse length (3.75 μs) and a relaxation delay time of 60 s; 16 free induction decay (FID) signals were accumulated. FID signals were multiplied by an exponential apodization function corresponding to a Lorentzian line broadening of 50 Hz. For ^{1}H analysis, a Bloch decay sequence was used, with a 90° pulse length (2.5 μs) and a relaxation delay time of 10 s; 16 FID signals were also accumulated. No exponential apodization function was applied to ^{1}H FID. The background signals from ^{1}H in the hardware were subtracted after matched spectrum on an empty rotor. ^{31}P and ^{1}H spectra were referenced to external 85% H_3PO_4 (0.0 ppm) and adamantane (1.8 ppm compared to TMS) as secondary reference sample, respectively. Peak assignment was based on previous solid-state nuclear magnetic resonance (NMR) studies using bone mineral, carbonate-containing apatite, and hydroxyapatite [6, 29–31].

Results

Cell Culture and General Mineralization Process

Long-term cultures of F-OST osteoblasts in the presence of osteogenic supplements (ascorbic acid and β-glycerophosphate) produced an extensive mineralized matrix. The supplements were added to the media when semiconfluence was reached at day 4 of culture. A fully confluent state was observed at about day 7. The first mineral deposits were noticed around day 9 of culture, appearing as small, discrete regions. These mineralizing areas gradually developed into larger, macroscopic nodular structures with heavier centers and different degrees of fusion with near neighbors (Fig. 1a). New deposits were seen arising in the course of culture; hence, nodules in different stages of development could be observed at the same culture time. The deposits were identified as mineralized regions by positive staining in black for phosphate (Fig. 1b) and red for calcium (Fig. 1c). A clear nodular staining pattern could be observed. Throughout culture time, the area occupied by mineral deposits increased significantly, extending to around 90% of the dish surface at day 28 (Fig. 1d). A lower rate of mineralization could be noticed in the last week of culture.

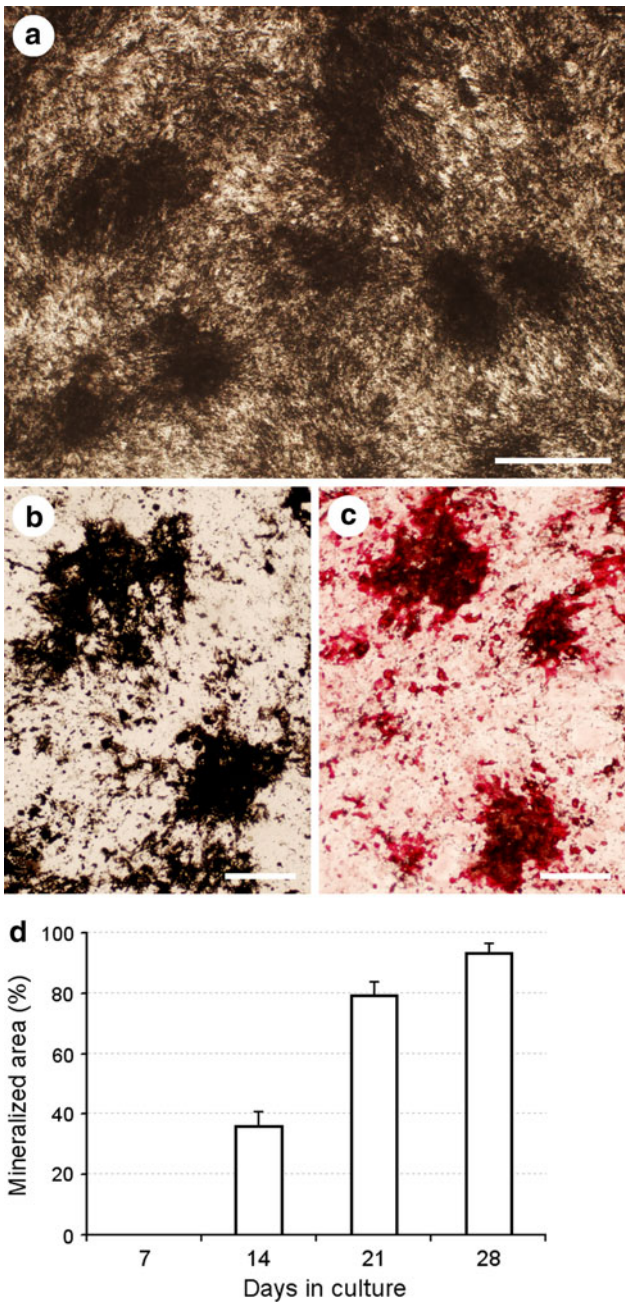

Fig. 1 General analysis of the mineralized cultures. **a** Light micrograph of unstained 28-day-old culture. Note the mineralizing nodules. **b** Light micrograph of 14-day-old culture stained using von Kossa's method. Phosphate deposits are shown in *black*. **c** Light micrograph of 14-day-old culture stained with nuclear fast *red*. Calcium deposits are shown in *red*. **d** Quantification of the area occupied by mineralizing regions after 7, 14, 21, and 28 days of culture. Note the significant increase throughout time, showing a lower mineralization rate in the last week of culture. *Scale bars* **a** 0.5 mm, **b** and **c** 0.15 mm (Color figure online)

Ultrastructural Analysis

Analysis of the mineralizing nodules assembled on F-OST osteoblast cultures using SEM presented numerous

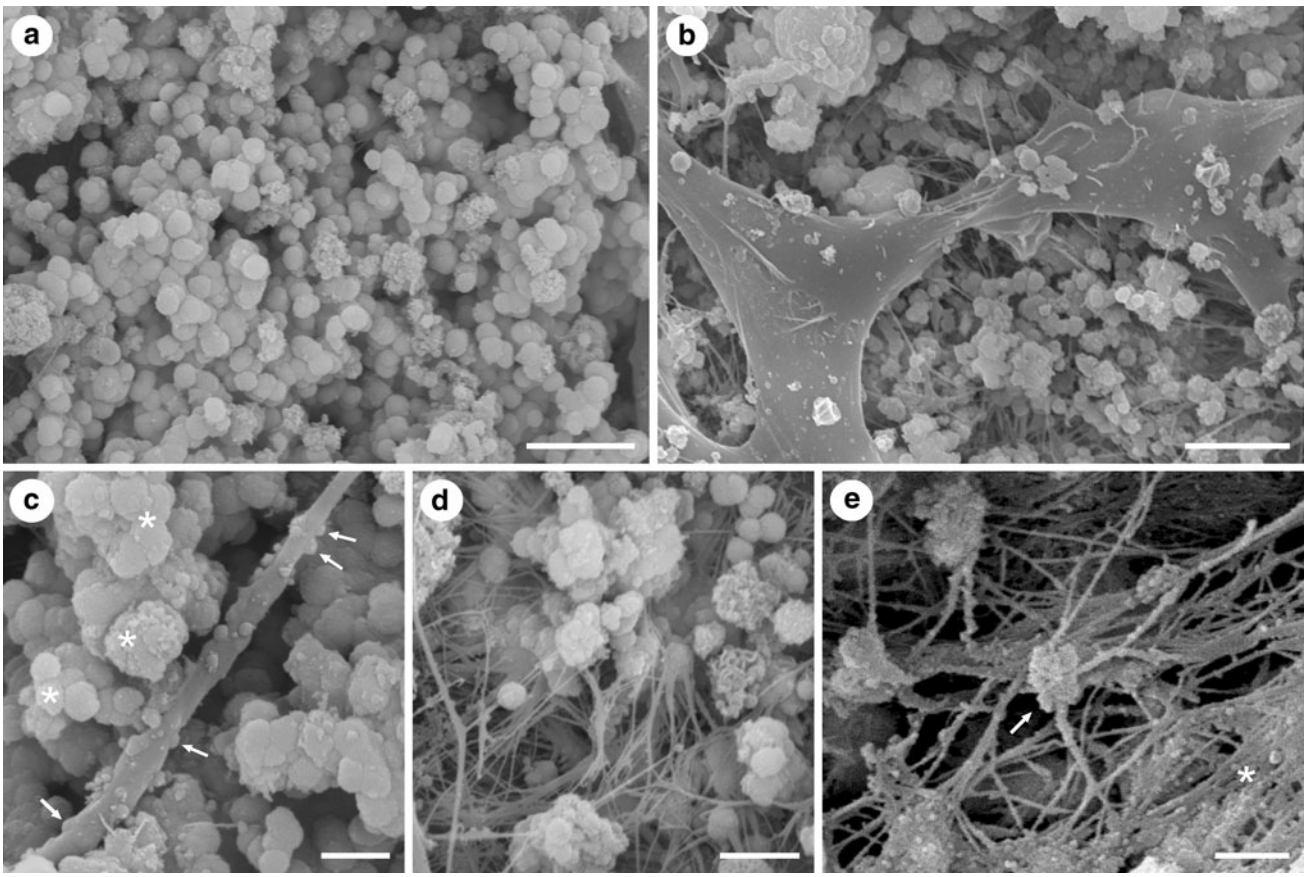

Fig. 2 SEM ultrastructural analysis of the mineralized cultures. **a** Globular accretions of about 1 μm in diameter were seen as the chief mineralization feature. **b** Accretions were mainly observed beneath the cells. **c** Note the groups of accretions presenting different degrees of coalescence (*asterisks*). Note also the small accretions with an average diameter of about 230 nm (varying from about 90 to 400 nm) associated with cell processes. Some of these accretions seem to be budding from the cell membrane (*arrows*). **d** Note the loosely packed arrays of collagen fibrils found in conjunction with accretions. **e** Note the mineralized fibrils, found in association with small deposits. These fibrils were often seen in bundles (*asterisk*) and/or in close contact with globular accretions (*arrow*). *Scale bars* **a** 5, **b** 10, **c** 2, **d** 3, **e** 2 μm

globular accretions of about 1 μm in diameter as its chief feature (Fig. 2a). These accretions were often seen beneath the cell layers, associated with a fibrous mesh (Fig. 2b). Many groups of globular accretions could be observed, presenting different degrees of coalescence: some in which it was possible to identify individual accretions and others in which its boundaries were completely indistinguishable (asterisks in Fig. 2c). These accretions appeared to be fusing with near neighbors forming larger mineralized features, which seemed to be gradually augmented by the incorporation of new accretions. Small accretions with an average diameter of about 230 nm (ranging from about 90 to 400 nm) could also be seen associated with cell processes (Fig. 2c). Some of these small accretions appeared to be budding from the cell membrane (arrows in Fig. 2c). The extensive fibrous mesh seen beneath the cell layers comprised arrays of loosely packed, randomly oriented collagen fibrils, usually found in conjunction with accretions (Fig. 2d). Mineralized fibrils were often observed, appearing in association with very small deposits (Fig. 2e). Some fibrils could be seen forming mineralized bundles with adjacent fibrils (asterisk in Fig. 2e) and/or in close contact with globular accretions (arrow in Fig. 2e).

Atomic force microscopic (AFM) analysis of the mineralized cultures confirmed the observations made using SEM. Beneath the cell layers, globular accretions with an average diameter of about 1 μm were often seen in conjunction with randomly oriented collagen fibrils (Fig. 3a). Many fibrils could be found closely around the accretions (Fig. 3b). In some regions of the fibrils, a banding-like pattern could be noticed, presenting an average periodicity between 55 and 85 nm. Arrays of fibrils displaying mineralized regions were also observed (Fig. 3c). The mineralized fibrils seemed to be engulfed by the mineral deposits. In these mineralized regions, the banding-like pattern of the fibrils appeared partially occluded. Small globular accretions could be found in association with cell processes (Fig. 3d), being very similar to those described

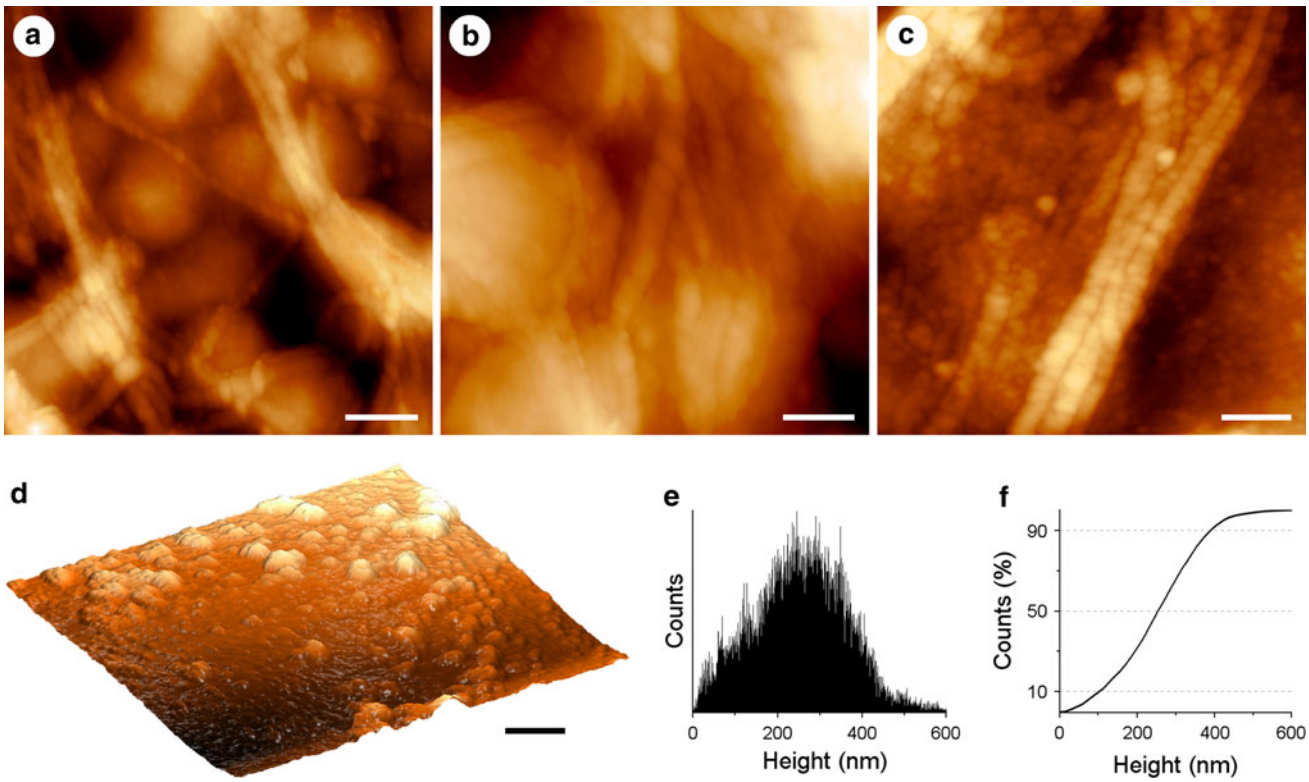

Fig. 3 AFM ultrastructural analysis of mineralized cultures. **a** Globular accretions with an average diameter of about 1 μm were often found beneath the cells, along collagen fibrils. **b** Fibrils could be seen closely around accretions. Note the banding-like pattern shown in some fibrils, displaying an average periodicity between 55 and 85 nm. **c** Note the arrays of fibrils presenting mineralized regions. Mineralized fibrils appeared to be engulfed by the mineral deposits. Note that the banding-like pattern seems partially occluded in these mineralized regions. **d** Three-dimensional image of a cell surface. Note the small globular accretions seemingly budding from the cell membrane, increasing in size, and coalescing. **e** Roughness analysis shows the average height of these small accretions about 250 nm. **f** Bearing ratio analysis shows about 80% of the accretions varying from 100 to 400 nm in height. *Scale bars* **a** 1, **b** 0.5, **c** 0.3, **d** 1 μm

using SEM. These features appeared to be budding from the membrane, increasing in size and coalescing, forming larger accretions. The average height of these small accretions was close to 250 nm (Fig. 3e), with about 80% ranging from 100 to 400 nm (Fig. 3f).

The ultrastructure of the mineralized cultures was further detailed using TEM. Many globular accretions and collagen fibrils were also observed (Fig. 4a). Some mineralized fibrils were found spatially near to the accretions (arrows in Fig. 4a). In some cases, crystallites apparently derived from the accretions could be seen in association with adjacent fibrils (arrowhead in Fig. 4a). The mineralized fibrils seemed to present crystallites both within its structure and on its surface. Groups of globular accretions could often be observed, describing a clear coalescence process (Fig. 4b). Moreover, small accretions seemed to be incorporating into larger ones (asterisks in Fig. 4a). The accretions were loaded with very small needle-shaped crystallites, mainly located on their periphery, presenting a radial arrangement (Fig. 4c). Some plate-shaped crystallites were also occasionally observed (arrows in Fig. 4c). The mineral crystallites often seemed to be superimposed on neighbors with the same orientation, resembling larger crystallites.

Mineral Phase Characterization

The mineral phase produced on F-OST osteoblast cultures was further characterized after removal of the organic components. The extracted mineral appeared on TEM as aggregates of nanometric plate- and needle-shaped crystallites, identified mainly on their periphery (Fig. 5a). As observed in the ultrastructural analysis using TEM, many neighbor crystallites with the same orientation seemed to be superimposed, giving the appearance of larger crystallites. The average Ca/P atomic ratio was determined at about 1.49 (standard deviation 0.06) using EDS analysis (inset in Fig. 5a). Investigating the mineral phase using HRTEM, a poorly crystalline arrangement of atoms was noticed, presenting small crystalline domains (arrow in Fig. 5b) often in conjunction with amorphous regions (asterisk in Fig. 5b). The mineral could be identified as hydroxyapatite by FFT analysis (inset in Fig. 5b), in which the dotted pattern corresponded to diffraction spots indexed

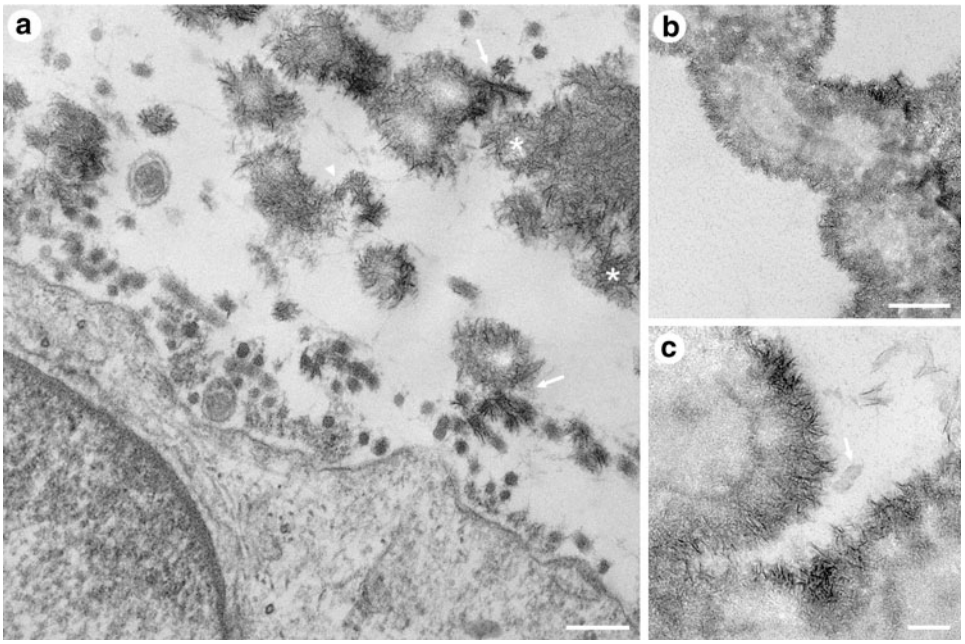

Fig. 4 TEM ultrastructural analysis of the mineralized cultures. **a** Globular accretions and collagen fibrils were often seen. Some mineralized fibrils were found close to accretions (*arrows*). Crystallites apparently derived from accretions could be noticed in association with adjacent fibrils (*arrowhead*). Note that crystallites seemed to be present within and on the surface of the mineralized fibrils. Some small globular accretions appeared to be incorporating into larger ones (*asterisks*). **b** Groups of globular accretions presenting a clear coalescence process were seen. **c** Accretions were loaded with very small needle-shaped crystallites. Note the higher content of crystallites on the periphery of the accretions, presenting a radial arrangement. Plate-shaped crystallites were occasionally noticed (*arrow*). *Scale bars* **a** 0.15, **b** 0.3, **c** 0.1 μm

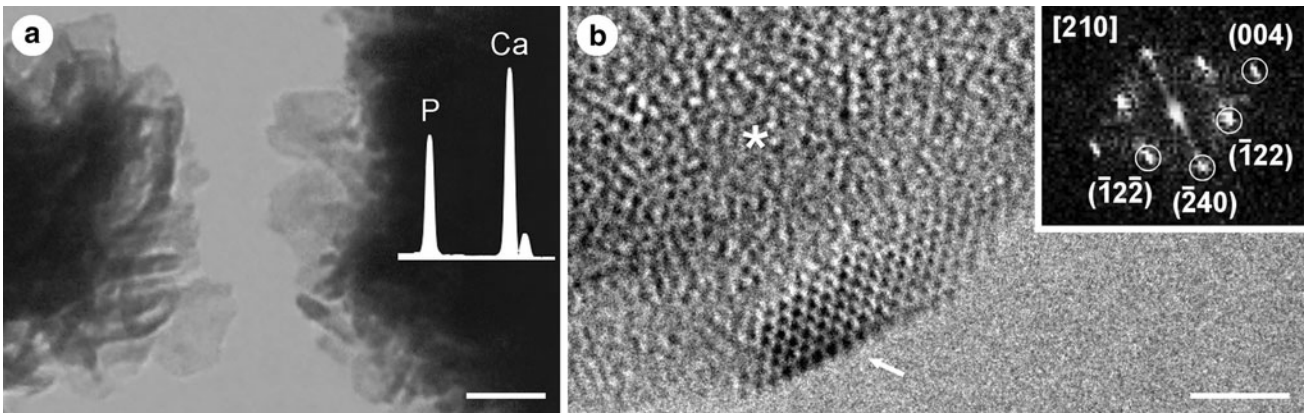

Fig. 5 Structural and elemental analysis of the extracted mineral. **a** TEM image. Note the nanometric plate- and needle-shaped crystallites seen on the periphery of mineral aggregates. *Inset* shows a typical EDS spectrum of the mineral. An average Ca/P atomic ratio of about 1.49 (standard deviation 0.06) was found. **b** HRTEM image. Note the small crystalline domain (*arrow*) along with an amorphous region (*asterisk*). *Inset* presents the FFT pattern of the crystalline domain. The mineral was identified as hydroxyapatite. The spots and zone axis are labeled. *Scale bars* **a** 30 and **b** 2 nm

as (004), (–122), (–240) and (–12–2) reflections from lattice planes within crystallites observed in the (210) zone axis.

The poorly crystalline nature of the mineral could also be noticed on the XRD pattern, which displayed generally broad peaks with low resolution (Fig. 6). The only mineral phase identified was hydroxyapatite, with the main observed diffraction peaks indexed as (002), (211), and (310) reflections (ICCD PDF 9-432). However, the broad asymmetric peak with high intensity around 30–35° 2θ may consist of four overlapping peaks, which could be assigned to the triplet for reflections (211), (112), and (300), with the (202) reflection appearing as a faint shoulder at 34° 2θ. The low-intensity broad peak around

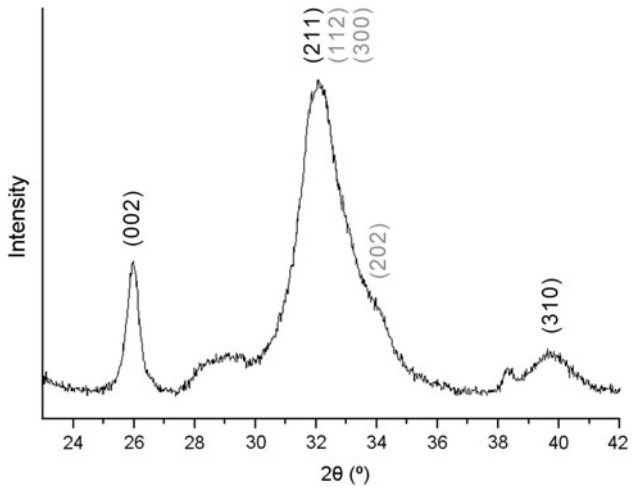

Fig. 6 XRD analysis of the extracted mineral. The XRD pattern is shown. The mineral was identified as hydroxyapatite. Note the poorly crystalline nature of the mineral, indicated by the generally broad peaks with low resolution. The main diffraction peaks are labeled. Values for the lattice parameters were $a = 9.435$ Å and $c = 6.860$ Å. The average crystallite size was about 20 nm long and 10 nm wide

28–30° 2θ may be attributed to the (102) and (210) reflections. To investigate the crystallographic properties of the apatite produced in culture, the lattice parameters and crystallite size were evaluated. The calculated values for the lattice parameters of the unit cells were as follows: $a = 9.435$ Å and $c = 6.860$ Å. The average crystallite size was estimated at about 20 nm in length along the c-axis and 10 nm in width perpendicular to the c-axis.

The isolated mineral was further identified as a poorly crystalline, carbonate-containing hydroxyapatite by FTIR (Fig. 7a, b). The triply degenerate $v_3PO_4^{3-}$ domain (1,200–900 cm^{-1}) was presented as a broad band with maxima at 1,034 cm^{-1} and a discrete shoulder around 1,095 cm^{-1}; the nondegenerate $v_1PO_4^{3-}$ domain (1,000–950 cm^{-1}) appeared as a clear peak at 961 cm^{-1}, partially overlapped with the $v_3PO_4^{3-}$ band; and the triply degenerate $v_4PO_4^{3-}$ domain (650–500 cm^{-1}) was resolved into two distinct peaks at 604 and 563 cm^{-1}. Carbonate domains appeared as noticeable bands for $v_3CO_3^{2-}$ (1,600–1,350 cm^{-1}) and $v_2CO_3^{2-}$ (890–850 cm^{-1}). Water bands were also present for v_1H_2O and v_3H_2O around 3,700–2,500 cm^{-1} and for v_2H_2O at 1,640 cm^{-1}. No bands for the OH groups were observed for the v_1OH^- or v_LOH^- domains at 3,572 and 630 cm^{-1}, respectively. Since the organic matrix was removed during mineral extraction, the main protein bands amide I (1,700–1,600 cm^{-1}) and amide II (1,600–1,500 cm^{-1}) were negligible. Deconvolution of phosphate and carbonate bands was performed in order to enhance the resolution of overlapping peaks. Analyses of

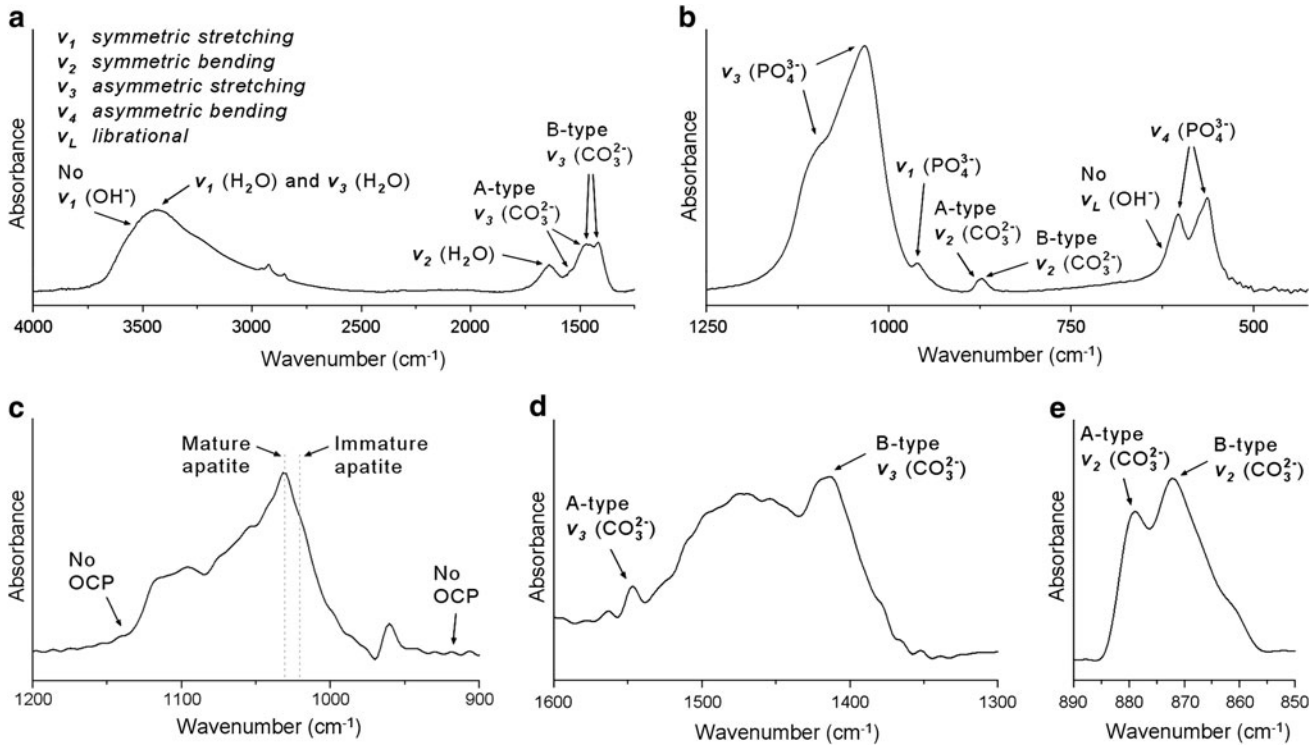

Fig. 7 FTIR analysis of the extracted mineral. **a**, **b** FTIR spectrum. The mineral was identified as poorly crystalline, carbonate-containing hydroxyapatite. The spectrum was divided to facilitate the observation of the phosphate bands; however, the relative absorbance is the same. **c** Deconvoluted $v_3PO_4^{3-}$ domain. Note the maturation degree of the apatite. **d** Deconvoluted $v_3CO_3^{2-}$ domain. **e** Deconvoluted $v_2CO_3^{2-}$ domain. Note the presence of CO_3^{2-} in both PO_4^{3-} (B-type) and OH (A-type) sites. The main peaks are labeled in all spectra

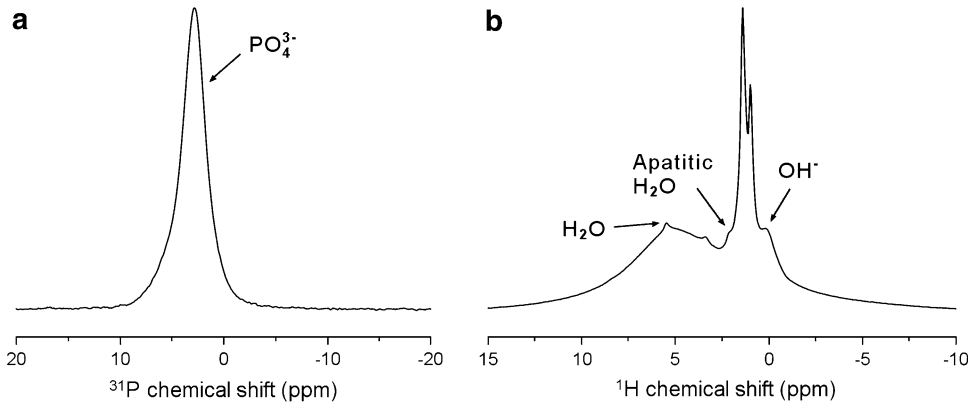

Fig. 8 Solid-state NMR analysis of the extracted mineral. **a** ^{31}P NMR spectrum. **b** ^{1}H NMR spectrum. The mineral was identified as hydroxyapatite containing structural water. Note the evident presence of isolated OH groups. Note also the apatitic water found occupying OH vacancies. The main peaks are labeled. The assignment of the unlabeled peaks is discussed in "Results" section

the $v_3PO_4^{-3}$ domain showed the peak for mature apatite at 1,030 cm^{-1} as the major band component, while the one for immature apatite at 1,020 cm^{-1} appeared only as a faint shoulder (Fig. 7c). Moreover, no band for octacalcium phosphate (OCP) was observed at 1,138 or 915 cm^{-1}. Carbonate peaks appear for substitutions both in phosphate (B-type carbonate) and OH (A-type carbonate) sites, with an apparent preference for B sites. Deconvolution of the $v_3CO_3^{2-}$ domain showed defined peaks for B-type carbonate at 1,416 cm^{-1} and for A-type at 1,547 cm^{-1} (Fig. 7d), while the $v_2CO_3^{2-}$ domain presented the B-type carbonate peak at 871 cm^{-1} and the A-type at 879 cm^{-1} (Fig. 7e). The absence of the labile carbonate peak at 866 cm^{-1} may reflect the advanced maturation degree of the apatite crystallites, although it could also be related to a minor loss of labile groups during mineral extraction.

The presence of orthophosphate in the isolated mineral was confirmed by solid-state ^{31}P NMR, appearing as a readily identifiable, characteristic peak at 2.8 ppm (Fig. 8a). No other phosphorus-bearing species were detected. The presence of OH ions and different types of water was evident in the ^{1}H NMR spectrum (Fig. 8b). The typical signal for isolated OH groups was observed as a clear peak at 0.1 ppm. The peaks at 1.4 and 0.9 ppm could be assigned to OH ions in hydrogen-bonding environments; however, they may also be related to residual matrix lipids not removed during mineral extraction [6]. The peak seen at 3.3 ppm might be assigned to P–OH groups on the surface of the crystallites. The water peak at 5.4 ppm could be assigned to bulk and loosely bound surface water but also to water molecules occupying vacancies within the crystallite lattice [6]. The peak at 2.2 ppm may be assigned to water molecules occupying isolated OH vacancies.

Discussion

F-OST osteoblast cultures achieved an extensive mineral formation, which presented definite similarities to physiological bone mineralization [1, 2, 5, 32]. In order to accelerate matrix development, the cells were cultured in a classic osteogenic medium containing 10 mM β-glycerophosphate, routinely used as a phosphate source in mineralizing cell culture systems [18]. Many groups using 10 mM β-glycerophosphate have described a bone-like mineralization in systems with different cell sources, including primary osteoblasts [16, 33], osteoblastic cell lines [19], and bone marrow stromal cells [34]. However, high levels of β-glycerophosphate can lead to a nonphysiological, dystrophic mineral deposition when occurring on an improper matrix since it may reflect the presence of alkaline phosphatase rather than the osteogenic properties of the culture [18, 21]. Thus, the mineralized matrix assembled under treatment with β-glycerophosphate must be carefully analyzed using a combination of physicochemical approaches in order to assure the occurrence of a physiological, bone-like mineralization [18]. In this study, the use of a large variety of methods allowed a detailed evaluation of the mineralized matrix assembled in F-OST osteoblast cultures. Systems with dystrophic mineral deposits were shown to present a diffuse mineralization pattern (without mineralizing nodules) [15], clumps of unidentified crystals, and absence of mineralized collagen fibrils and apatite formation [19]. As further discussed in this section, the ultrastructure of the matrix and the extracted mineral phase described in the present study shared many characteristics with native bone tissue, rather than with dystrophic mineralization. Since F-OST osteoblasts were previously shown to produce mineralizing nodules in the absence of β-glycerophosphate [22], the use of osteogenic medium seemed to act mainly by accelerating matrix development while keeping the formation of mineralizing bone-like nodules similar to those described by others [15, 35]. Incidentally, cultures that achieve a nodular mineralization pattern were suggested to be more suitable for evaluating osteoinductive properties of biomaterials [20].

The ultrastructure of the mineralized F-OST osteoblast cultures showed several characteristics of native bone [1, 32] and bone-like mineralization [15, 33], presenting globular accretions loaded with mineral crystallites, an

extensive collagenous framework, and mineralized fibrils. Globular accretions were reported with different names in many studies with bone (such as calcospherites [12], calcified microspheres [32], calcifying nodules [36], calcospherulites [37]) and mineralized cultures (such as globular accretions [15], calcified spheres [17], globular masses [33], calcified nodules [38]). In the present study, the term "globular accretion" has been adopted for these calcium phosphate-containing globular bodies, which undergo gradual growth and coalescence to form larger structures.

The development of the globular accretions may be related to matrix vesicles. These vesicles arise by budding from the plasma membrane of cells and play an essential role in early mineralization [8, 9]. Throughout maturation, these vesicles increase in size, acting as initial sites for nucleating apatite crystallites, which arrange in radial clusters close to their periphery [8]. These crystallites terminally rupture the vesicles membrane, forming larger globular accretions that coalesce into mineralization fronts [12, 14]. The formation of these accretions may be augmented by matrix vesicle aggregation [37]. A similar mineralization cascade may occur in F-OST osteoblast cultures. For example, the small accretions associated to cell surfaces resemble early matrix vesicles budding from the plasma membrane, while those presenting innumerable needle-shaped crystallites disposed in a radial pattern close to their periphery may represent a stage in which the vesicle membrane has been terminally ruptured. The coalescence of globular accretions could illustrate the formation of mineralization fronts. The origin of the accretions might also be related to NCP aggregates. These aggregates are often seen as organic substructures (crystal ghosts) of globular accretions in bone [10] and were also suggested to be related to the accretions found in culture systems [11, 17]. The increase of the accretion may be augmented by the fusion of matrix vesicles with NCP aggregates [11].

The collagenous matrix found in F-OST osteoblast cultures resembled that of woven bone, presenting loosely packed, randomly oriented collagen fibrils [1]. The presence of numerous globular accretions may also indicate similarities to woven bone, suggesting the existence of high amounts of matrix vesicles and NCP, considered the chief feature in the mineralization front of woven bone [3, 14]. The mineralized matrix found in culture systems usually presents a woven bone-like structure [21, 39].

Mineralized collagen fibrils are accepted as the basic building block common to all bone tissues [1]. Mineralized fibrils observed in F-OST osteoblast cultures resemble those found in the bone-like matrix described in other culture systems [17, 33, 34]. In some cases, mineralization of the collagen fibrils may be induced by matrix vesicles and/or NCP [8, 37]. This scenario may be represented by the close association found between some globular accretions and mineralized fibrils in F-OST osteoblast cultures.

In order to better characterize the mineral phase, the organic matrix is often removed. Different methods can achieve the degradation of the organic components and a successful mineral extraction, e.g., based on sodium hypochlorite [23, 24] and hydrazine [40]. However, the extraction procedures may lead to different degrees of change in the mineral composition and structure [29, 40]. Mahamid et al. [24] recently described the isolation of apatite crystallites from the fin bones of zebrafish using a sodium hypochlorite treatment. The authors tested the extraction procedure on highly metastable amorphous calcium phosphate (ACP) and found that it did not alter the mineral phase. In the present study, the mineral extraction was based mainly on their method. The procedure was performed in continuous motion, which has been shown to prevent the dissolution of bone apatite crystallites subjected to sodium hypochlorite treatment [23]. However, it is important to note that some amorphous mineral phases may have been dissolved during extraction and washes. A minor loss of labile groups is also plausible, similar to that described in the bone apatite isolated using nonaqueous hydrazine treatment [40]. Moreover, since it is conceivable that some very small crystallites could have been dissolved during extraction [23], leading to a relative increase in the proportion of larger crystallites, it is also important to consider that the average crystallite size of the apatite found in this study may be slightly overestimated. As further discussed below, the mineral extracted from F-OST osteoblast cultures was very similar to that found in native bone, presenting typical characteristics described for bone apatite, e.g., regarding crystallite shape and size (width and length) [40], Ca/P atomic ratio [2, 41], crystallinity degree [7], unit cell lattice parameters (a and c) [26], amount of isolated OH groups [6, 29], and presence of carbonate substitutions [27] and apatitic water [6]. Thus, it is proposed that, although some degree of change may have occurred, the overall mineral phase analyzed in this study was not significantly altered by the extraction procedure.

The earliest precursor for bone apatite may be an ACP [24]. It was previously proposed that the transition of ACP into apatite may occur through intermediate phases, namely an OCP or OCP-like phase [42]. However, the nature of the precursor phase(s) of the biological apatite found in bone is still under some controversy, especially regarding the existence of a transient OCP or OCP-like phase [7]. In this context, it is conceivable that the amorphous regions found in the mineral produced in F-OST osteoblast cultures may act as precursors for apatite crystallite formation. As was reported in bone samples [24] and mineralized cultures [16], OCP was not identified in this study.

The nonstoichiometric nature of bone apatite can be explained by the existence of substitution (such as carbonate and HPO_4) and vacancies (such as in Ca and OH sites) in the crystallite structure [5, 7]. Carbonate can be found replacing both phosphate (B-type carbonate) and OH (A-type carbonate) groups in bone [4, 27] and culture systems [16], with a higher content in phosphate sites [5]. A similar carbonate distribution was observed in the mineral phase produced in F-OST osteoblast cultures. Water molecules can also occupy some OH channels, forming hydrogen bonds to surrounding phosphate, carbonate, and/or OH ions and helping to stabilize the crystallite structure [6]. This type of apatitic water was also found in the mineral phase produced in F-OST osteoblast cultures.

The Ca/P atomic ratio of bone mineral varies from about 1.49 in embryonic woven bone to values close to or above 1.67 in adult bone [41, 43]. The Ca/P atomic ratio found in the mineral phase produced in F-OST osteoblast cultures was very similar to that described in woven bone, which is in agreement with the ultrastructural characterization discussed above. Bone apatite presents an OH content of about 20% of the expected amount for stoichiometric hydroxyapatite [29], which is often not detected in FTIR spectra of native bone [44] and mineralized cultures [16], including F-OST osteoblast cultures. However, the presence of isolated OH groups in the mineral phase produced in F-OST osteoblast cultures was evident in solid-state ^1H NMR spectra, similar to previous reports for bone apatite [6, 29]. The nondetection of OH groups in the FTIR spectra may be related to the existence of hydrogen bonds between some OH ions and water molecules present within OH channels [6, 44].

Bone mineral comprises a polycrystalline material, presenting nanometric crystallites with different sizes and degrees of orientation [2, 13]. The shape of the crystallites produced in F-OST cultures resembles that described in bone [13, 40], characterized as thin, irregular plates that appear needle-like when oriented edge-on. Besides the crystalline domains, bone mineral also contains many amorphous regions, being characterized as a poorly crystalline material [2, 5]. A similar poorly crystalline nature was observed in the mineral produced in F-OST osteoblast cultures. Bone apatite has a hexagonal crystallite structure (space group $P6_3/m$) presenting lattice parameter values about $a = 9.419$ Å and $c = 6.882$ Å [2, 26]. The lattice parameters of the apatite produced in F-OST osteoblast cultures shared similar values. The bone apatite crystallites present a wide range of dimensions from about 10 to 100 nm, with the majority shorter than 45 nm in length [23, 40]. The average crystallite size described in F-OST osteoblast cultures was very similar to that previously reported in bone [26, 40].

Despite the similarities to woven bone observed in F-OST osteoblast cultures, the mineral phase presented a maturation degree close to mature apatite. Corresponding results were described in other culture systems, and a reasonable hypothesis was proposed [16]. Embryonic woven bone presents a rapid remodeling rate, resulting in a high proportion of newly deposited, immature crystallites; in contrast, mineralization in culture systems occurs without mineral resorption, leading to an accumulation of crystallites that are allowed to mature over time in culture [7, 16]. Since the mineralization rate described in F-OST osteoblast cultures decrease after about 21 days, at the end of the culture period there may be a higher proportion of older versus newly deposited crystallites, resulting in an overall maturation degree closer to mature than immature apatite.

The mineralized matrix assembled in F-OST osteoblast cultures under osteogenic conditions (50 µg/ml ascorbic acid and 10 mM β-glycerophosphate) presented many ultrastructural and mineral phase characteristics similar to those described in native bone and in the bone-like matrix produced in other culture systems. The ultrastructure of the matrix presented several features described in woven bone, such as extensive arrays of loosely packed, randomly oriented collagen fibrils and innumerable globular accretions loaded with mineral crystallites. These accretions seem to be mainly related to matrix vesicles, representing different stages of their mineralization cascade. Many mineralized collagen fibrils were also observed, often found in close association with accretions, suggesting a relationship between these two features and possibly their mineralization processes. The mineral phase produced in culture was extracted using a sodium hypochlorite treatment and characterized in detail, presenting many similarities with the apatite found in native bone. The mineral was described as a poorly crystalline, nonstoichiometric apatite containing carbonate substitutions on both phosphate and OH sites. The crystallites' shape and size and the unit cell dimensions were also typical of bone apatite. Furthermore, the presence of small amounts of isolated OH groups was observed. To our knowledge, this study presents some of the first evidence of isolated OH groups in the bone-like apatite produced in cell culture systems. In conclusion, F-OST osteoblast cultures may provide a good model not only to investigate fundamental bone mineralization processes but also to contribute in related studies, such as the biological evaluation of biomaterials and the effects of drugs on the bone apatite structure.

Acknowledgments The authors gratefully acknowledge COPPE/UFRJ for the SEM facilities and technical support, LNLS for the HRTEM facilities, M. M. Medeiros (ICB/UFRJ) for her support in electron microscopic analysis, F. P. Almeida (IMPPG/UFRJ) for his assistance in SEM analyses, J. Gomes Filho (CBPF) for his

contribution in AFM analysis, V. C. A. Moraes and V. A. Ferraz (CBPF) for their support in the XRD analyses, and C. L. R. Fragoso for his assistance in the FTIR analyses. This study was supported by CNPq, CAPES, FAPERJ, and FINEP Brazilian agencies.

References

1. Weiner S, Wagner HD (1998) The material bone: structure–mechanical function relations. Annu Rev Mater Sci 28:271–298
2. Dorozhkin SV (2009) Calcium orthophosphates in nature, biology and medicine. Materials 2:399–498
3. Nanci A (1999) Content and distribution of noncollagenous matrix proteins in bone and cementum: relationship to speed of formation and collagen packing density. J Struct Biol 126(3): 256–269
4. Pasteris JD, Wopenka B, Valsami-Jones E (2008) Bone and tooth mineralization: why apatite? Elements 4:97–104
5. Cazalbou S, Combes C, Eichert D, Rey C (2004) Adaptative physico-chemistry of bio-related calcium phosphates. J Mater Chem 14:2148–2153
6. Wilson EE, Awonusi A, Morris MD, Kohn DH, Tecklenburg MM, Beck LW (2006) Three structural roles for water in bone observed by solid-state NMR. Biophys J 90(10):3722–3731
7. Rey C, Combes C, Drouet C, Glimcher MJ (2009) Bone mineral: update on chemical composition and structure. Osteoporos Int 20(6):1013–1021
8. Landis WJ, Silver FH (2002) The structure and function of normally mineralizing avian tendons. Comp Biochem Physiol A Mol Integr Physiol 133(4):1135–1157
9. Anderson HC (2003) Matrix vesicles and calcification. Curr Rheumatol Rep 5(3):222–226
10. Bonucci E (2002) Crystal ghosts and biological mineralization: fancy spectres in an old castle, or neglected structures worthy of belief? J Bone Miner Metab 20(5):249–265
11. Midura RJ, Wang A, Lovitch D, Law D, Powell K, Gorski JP (2004) Bone acidic glycoprotein-75 delineates the extracellular sites of future bone sialoprotein accumulation and apatite nucleation in osteoblastic cultures. J Biol Chem 279(24):25464–25473
12. Sela J, Gross UM, Kohavi D, Shani J, Dean DD, Boyan BD, Schwartz Z (2000) Primary mineralization at the surfaces of implants. Crit Rev Oral Biol Med 11(4):423–436
13. Weiner S, Traub W (1992) Bone structure: from angstroms to microns. FASEB J 6(3):879–885
14. Bonucci E (2007) The organic–inorganic relationships in calcifying matrices. In: Biological calcification: normal and pathological processes in the early stages. Springer, Berlin, pp 443–489
15. Parker E, Shiga A, Davies JE (2000) Growing human bone in vitro. In: Davies JE (ed) Bone engineering. Em Squared, Toronto, pp 63–77
16. Kuhn LT, Wu Y, Rey C, Gerstenfeld LC, Grynpas MD, Ackerman JL, Kim HM, Glimcher MJ (2000) Structure, composition, and maturation of newly deposited calcium-phosphate crystals in chicken osteoblast cell cultures. J Bone Miner Res 15(7): 1301–1309
17. Barragan-Adjemian C, Nicolella D, Dusevich V, Dallas MR, Eick JD, Bonewald LF (2006) Mechanism by which MLO-A5 late osteoblasts/early osteocytes mineralize in culture: similarities with mineralization of lamellar bone. Calcif Tissue Int 79(5): 340–353
18. Boskey AL, Roy R (2008) Cell culture systems for studies of bone and tooth mineralization. Chem Rev 108(11):4716–4733
19. Bonewald LF, Harris SE, Rosser J, Dallas MR, Dallas SL, Camacho NP, Boyan B, Boskey A (2003) von Kossa staining alone is not sufficient to confirm that mineralization in vitro represents bone formation. Calcif Tissue Int 72(5):537–547
20. Declercq HA, Verbeeck RM, De Ridder LI, Schacht EH, Cornelissen MJ (2005) Calcification as an indicator of osteoinductive capacity of biomaterials in osteoblastic cell cultures. Biomaterials 26(24):4964–4974
21. Hoemann CD, El-Gabalawy H, McKee MD (2009) In vitro osteogenesis assays: influence of the primary cell source on alkaline phosphatase activity and mineralization. Pathol Biol (Paris) 57(4):318–323
22. Balduino A, Hurtado SP, Frazão P, Takiya CM, Alves LM, Nasciutti LE, El-Cheikh MC, Borojevic R (2005) Bone marrow subendosteal microenvironment harbours functionally distinct haemosupportive stromal cell populations. Cell Tissue Res 319(2):255–266
23. Weiner S, Price PA (1986) Disaggregation of bone into crystals. Calcif Tissue Int 39(6):365–375
24. Mahamid J, Sharir A, Addadi L, Weiner S (2008) Amorphous calcium phosphate is a major component of the forming fin bones of zebrafish: indications for an amorphous precursor phase. Proc Natl Acad Sci USA 105(35):12748–12753
25. Shih WJ, Wang MC, Hon MH (2005) Morphology and crystallinity of the nanosized hydroxyapatite synthesized by hydrolysis using cetyltrimethylammonium bromide (CTAB) as a surfactant. J Cryst Growth 275(1–2):2339–2344
26. Meneghini C, Dalconi MC, Nuzzo S, Mobilio S, Wenk RH (2003) Rietveld refinement on X-ray diffraction patterns of bioapatite in human fetal bones. Biophys J 84(3):2021–2029
27. Rey C, Collins B, Goehl T, Dickson IR, Glimcher MJ (1989) The carbonate environment in bone mineral: a resolution-enhanced Fourier transform infrared spectroscopy study. Calcif Tissue Int 45(3):157–164
28. Rey C, Shimizu M, Collins B, Glimcher MJ (1991) Resolution-enhanced Fourier transform infrared spectroscopy study of the environment of phosphate ion in the early deposits of a solid phase of calcium phosphate in bone and enamel and their evolution with age: 2. Investigations in the v_3PO_4 domain. Calcif Tissue Int 49(6):383–388
29. Cho G, Wu Y, Ackerman JL (2003) Detection of hydroxyl ions in bone mineral by solid-state NMR spectroscopy. Science 300(5622):1123–1127
30. Kaflak-Hachulska A, Samoson A, Kolodziejski W (2003) 1H MAS and 1H–31P CP/MAS NMR study of human bone mineral. Calcif Tissue Int 73(5):476–486
31. Kolmas J, Kolodziejski W (2007) Concentration of hydroxyl groups in dental apatites: a solid-state 1H MAS NMR study using inverse 31P–1H cross-polarization. Chem Commun (Camb) 42:4390–4392
32. Carter DH, Hatton PV, Aaron JE (1997) The ultrastructure of slam-frozen bone mineral. Histochem J 29(10):783–793
33. Nanci A, Zalzal S, Gotoh Y, McKee MD (1996) Ultrastructural characterization and immunolocalization of osteopontin in rat calvarial osteoblast primary cultures. Microsc Res Tech 33(2):214–231
34. Rohde M, Mayer H (2007) Exocytotic process as a novel model for mineralization by osteoblasts in vitro and in vivo determined by electron microscopic analysis. Calcif Tissue Int 80(5): 323–336
35. Bhargava U, Bar-Lev M, Bellows CG, Aubin JE (1988) Ultrastructural analysis of bone nodules formed in vitro by isolated fetal rat calvaria cells. Bone 9(3):155–163
36. Lowe J, Bab I, Stein H, Sela J (1983) Primary calcification in remodeling haversian systems following tibial fracture in rats. Clin Orthop Relat Res 176:291–297
37. Midura RJ, Vasanji A, Su X, Wang A, Midura SB, Gorski JP (2007) Calcospherulites isolated from the mineralization front of

bone induce the mineralization of type I collagen. Bone 41(6):1005–1016
38. Ecarot-Charrier B, Shepard N, Charette G, Grynpas M, Glorieux FH (1988) Mineralization in osteoblast cultures: a light and electron microscopic study. Bone 9(3):147–154
39. Majeska RJ, Gronowicz GA (2002) Current methodologic issues in cell and tissue culture. In: Bilezikian JP, Raisz LG, Rodan GA (eds) Principles of bone biology. Academic Press, San Diego, pp 1529–1541
40. Kim HM, Rey C, Glimcher MJ (1995) Isolation of calcium-phosphate crystals of bone by non-aqueous methods at low temperature. J Bone Miner Res 10(10):1589–1601
41. Cazalbou S, Combes C, Eichert D, Rey C, Glimcher MJ (2004) Poorly crystalline apatites: evolution and maturation in vitro and in vivo. J Bone Miner Metab 22(4):310–317
42. Crane NJ, Popescu V, Morris MD, Steenhuis P, Ignelzi MA Jr (2006) Raman spectroscopic evidence for octacalcium phosphate and other transient mineral species deposited during intramembranous mineralization. Bone 39(3):434–442
43. Rey C, Hina A, Tofighi A, Glimcher MJ (1995) Maturation of poorly crystalline apatites: chemical and structural aspects in vivo and in vitro. Cells Mater 5(4):345–356
44. Rey C, Miquel JL, Facchini L, Legrand AP, Glimcher MJ (1995) Hydroxyl groups in bone mineral. Bone 16(5):583–586